Electrocatalytic activity of undoped and Mn-doped Zn(S,Se)-carbon nanocomposites

Michał Kaczmarek · Michael Bredol

Abstract Electrocatalytic materials for applications, e.g. in fuel cells are often composites of (conducting) carbon variants and nanosized metal particles, typically from the family of platinum or nickel. They share some common problems (most notably a tendency to agglomeration and poisoning, e.g. by CO or H_2), which prevent their use in contact with, e.g. raw biogenic methane or ethanol. Highly purified fuels or reformation to hydrogen are therefore necessary for such purposes. As a potential alternative, this study describes electrocatalytic activity of composites of undoped and Mn-doped Zn(S,Se) nanoparticles and carbon in contact with ethanol. The results on ethanol oxidation on such electrodes in short-circuit mode are reported, as well as values for the open circuit voltage achieved so far. The focus of this report is the variation of the Se/S ratio in mixed nanocrystals of ZnS and ZnSe. The influence on the electrocatalytic activity by the varying band gap energy and absolute positions of the electronic levels of the doped as well as undoped chalcogenide nanoparticles is reported.

Introduction

Composites fabricated from nanoscaled ZnS and various organic and inorganic hosts have been described in the recent past by a variety of authors, mostly for optical applications [1–7]. Recently, ZnSe found much attention,

M. Kaczmarek · M. Bredol (✉)
Department of Chemical Engineering, Fachhochschule Münster, Stegerwaldstraße 39, 48565 Steinfurt, Germany
e-mail: bredol@fh-muenster.de

M. Kaczmarek
e-mail: michal.kaczmarek@fh-muenster.de

since its band gap energy is smaller than that of ZnS and only slightly larger than visible light; in Cu- or Mn- doped form it might therefore be a replacement for toxic "quanum dot" materials like CdSe and CdTe [8]. However, the electrocatalytic activity of II–VI materials, especially ZnS, is a field often neglected, although these materials may be chemically quite stable and have proven photocatalytic activity with organic materials [9, 10], as exemplified for instance also in recent reports using nanosized morphologies [11, 12]. On the other hand, catalysts for direct ethanol consumption in fuel cells are still in short supply; the metallic variants are meanwhile quite complicated systems [13, 14], but still are easily poisoned by intermediates like CO or contaminants like H_2S. Moreover, the literature now contains a huge number of different recipes to prepare II–VI semiconductor particles in active nanoparticulate form, modified by various ligands. Preparation procedures are not restricted to high boiling (organic) solvents, rather a variety of approaches using aqueous chemistry have been demonstrated as well for some time now [15]. In this article, we will discuss mixed crystals of ZnS and ZnSe and their electrocatalytic activity in the presence of ethanol. Approaches for the synthesis of the end members of mixed nanocrystals of such materials are taken from the recent work of Wang et al. [8] and have been modified for the preparation of mixed crystals. For composites of carbon and pure ZnS nanoparticles, electrocatalytic activity in the presence of ethanol has already been demonstrated by our group [16], thus this report will extend the study to mixed crystals of ZnS and ZnSe and the influence of such alloying on the electrocatalytic behaviour.

Zn(S,Se) has only low electronic conductivity, and therefore a conductive support is needed. Carbon variants are especially attractive, since they combine chemical robustness against aggressive acidic electrolytes with

sufficient electronic conductivity. Many special carbon-based materials are meanwhile available for electrochemical applications [17], but for this study a simple mixture of activated carbon and conductive carbon paste deposited on conductive glass (covered with indium tin oxide, ITO) has been used throughout all experiments as conductive matrix.

ZnS and ZnSe nanoparticles may easily be doped with Mn^{2+} or Cu^+ and then turn into luminescent nanoparticles. From a practical point of view, the presence of Mn^{2+}-doped particles thus can easily be detected by UV-illumination during the various stages of preparation of nanocomposites of these materials. Moreover, shifts in band gap energy can simply be measured by observation of excitation spectra monitored at Mn^{2+} emission. On the other hand, Mn is thought to be present on the surface of doped nanoparticles in quite high proportions and thus might influence the catalytic behaviour. This study therefore compares the catalytic activity of Mn-doped Zn(S,Se) with undoped material to find out the relative influence of shifts in band gap energy and position of conduction and valence bands as compared to the potential presence of Mn^{2+} on the surface of the particles.

From a theoretical point of view, band gap energies ($E_{g,observed}$) and absolute positions of band edges (E_{VB} for the valence band, E_{CB} for the conduction band) can be estimated as a function of particle size by the effective mass approach, as introduced by Brus [18]. Effective mass in this context is the mass that a charged particle inside the crystal would have in vacuum for the same response to electric or magnetic fields, here expressed in units of the ordinary electron mass (m_e^* for the electron, m_h^* for the hole). These simple concepts are still useful today, e.g. in recent work by Jaseniak et al. [19] to estimate size-dependent positions of band edges ($E_{g,bulk}$ is the band gap of large, ideal crystals, $E_{CB,bulk}$ the conduction band edge in such crystals):

$$E_{CB} = E_{CB,bulk} + \left(E_{g,observed} - E_{g,bulk}\right)\left(\frac{m_h^*}{m_h^* + m_e^*}\right) \quad (1)$$

$$E_{VB} = E_{CB} - E_{g,observed} \quad (2)$$

In ZnS and ZnSe, the effective mass of the hole m_h^* is about four times larger than m_e^*. According to Eq. 1, increases in band gap energy with decreasing particle size thus are mostly realized by an increase of the energy of the conduction band edge, whereas the position of the valence band edge does not vary that much.

For the parent (bulk) materials, van de Walle and Neugebauer [20] adjusted these edges on the electrochemical scale, using DFT calculations to indicate that the conduction band edge of bulk ZnSe is to be expected at lower energies than the one of ZnS, whereas the valence band edge of ZnSe is to be found at higher energy levels, when compared to ZnS. Fabricating mixed nanocrystals of ZnS and ZnSe thus means that the conduction band edge is shifted systematically to
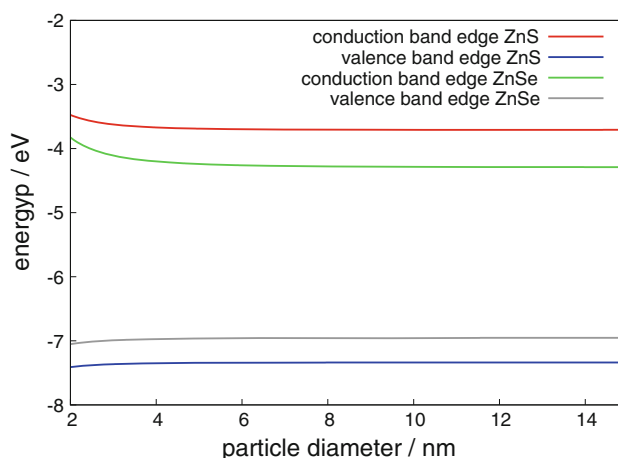

Fig. 1 Positions of conduction band edges and valence band edges for ZnS and ZnSe, as a function of particle diameter (schematically, as estimated from Eq. 1, relative to vacuum level)

higher energies by the particle size effect (at least when the region of weak confinement is reached), whereas alloying with ZnSe does reverse this trend, as compared to pure ZnS (see Fig. 1 for a sketch of the situation, using data from [20] and references therein). Since electrocatalytic electron exchange most probably proceeds via the conduction band of the chalcogenides, a marked influence on the catalytic behaviour by alloying is expected.

Another issue is the necessary presence of stabiliziers on the surface of the nanoparticles to prevent aggregation and precipitation. These ligands might act as a barrier against charge transfer and thus cause electrochemical overvoltages. Therefore, the ligands should be as small as possible with regard to its proven high adsorptive power to zinc chalcogenides, mercaptopropionic acid (MPA) was selected for this study [21]. The resulting hydrophilic particles can easily be dispersed in water and introduced into the hydrophilic environment of activated carbon.

All nanoparticles were prepared from aqueous solution under ambient pressure. Since ZnS and ZnSe have high melting temperatures, crystal quality under these conditions is limited. On the other hand, technical application will only be possible if particles can be fabricated by scalable processes, typically with water as solvent. In order to guarantee comparable crystal quality for experiments in this study, all nanoparticles were made by the same process; variations in sulphide to selenide ratio were set before particle preparation in the chalcogenide precursor solution.

Experimental

All chemicals were used as received without further purification. Synthesis of Zn(S,Se):Mn quantum dots was

adopted from a literature process [8]. For doped samples, 2 mol% of Mn (with respect to Zn) was added during synthesis.

The necessary chalcogenide precursor solution of $NaH(Se,S)$ was prepared in analogy to methods for NaHSe [22] and NaHTe [23] solutions. Under flowing N_2 atmosphere, 20 mL of 0.05 M NaOH was reacted with a mixture of gaseous H_2S and H_2Se, generated by complete reaction of intimate mixtures of solid Al_2Se_3 and FeS with H_2SO_4 (10%); Al_2Se_3 and FeS were used in a 1.7-fold excess as calculated from the amount of Zn^{2+} to be precipitated. After reaction, the solution was bubbled with N_2 for 30 min to remove any traces of H_2S and H_2Se in the precursor solution.

The freshly prepared chalcogenide precursor solution was added to an aqueous solution of MPA at pH = 11.2; in case of Mn-doped nanocrystals, this solution contained $MnCl_2$ as well to form $Mn(S,Se)$-containing nuclei before $Zn(S,Se)$ precipitation. All operations were performed under N_2 atmosphere. In a typical experiment, 0.4 mL of $MnCl_2$ solution (0.0125 M) and 0.52 mL of stabilizer (MPA) were loaded into a three-neck flask fitted with a septum, and pH was adjusted to 11.2 with 1 M NaOH. The solution was than degassed for 30 min by bubbling with nitrogen. 2.5 mL of freshly prepared oxygen-free 0.05 M $NaH(Se,S)$ solution was injected under vigorous stirring, and the solution was refluxed at 100 °C for 40 min in N_2 atmosphere. 20 mL of $Zn(NO_3)_2$ (0.0125 M) was added dropwise, and the mixture was refluxed again for 5 h under N_2. Finally, the product was cooled down, precipitated with ethanol, centrifuged and dried in vacuum.

The resulting powders were characterized by optical spectroscopy (*Shimadzu* fluorometer), dynamic light scattering (DLS, *Malvern*) and X-ray diffraction (XRD, *Rigaku*).

Nanocomposite carbon/$Zn(S,Se)$ electrodes were prepared essentially as described previously [16]. In short, activated carbon powder (*Merck*) was mixed with a dispersion of $Zn(S,Se)$ nanoparticles in water and dried. The resulting powder was mixed with carbon paste (*DuPont*) and applied to ITO-substrates by tape-casting and subsequent baking. Of course also other carbon variants should be possible; there are, e.g. already reports of ZnS nanoparticles conjugated to carbon nanotubes [24]. The final electrodes contained 15% nanoparticles by weight. Blank experiments were either performed with electrodes made from carbon paste and activated charcoal, but without $Zn(S,Se)$ nanoparticle, or with glass electrodes sputtered with indium tin oxide (ITO) to exclude influence by any metallic component.

All electrochemical measurements were made at room temperature using a *Zahner IM6* electrochemical work station.

Experimental fuel cells were constructed using a Fe^{3+}/Fe^{2+}/Pt oxidative counter electrode with equal ionic activities of Fe^{3+} and Fe^{2+}. The half cells were connected by a small glass membrane (diameter 1 mm) and operated either current-free (determination of open-circuit voltage V_{oc}) or in short-circuit mode (determination of short-circuit current I_{sc}) by the *Zahner IM6* in galvanostatic or potentiostatic mode, respectively. The whole electrochemical system was bubbled with N_2 during operation. Electrolyte in contact with the experimental electrode in all cases was 1m KNO_3 at a pH of 2–3. In order to protect the electrodes against oxidation of the $Zn(S,Se)$ by the counter electrode, the electrolyte did always contain ethanol (10% by volume).

Results and discussion

$Zn(S,Se)$ nanopowders as synthesized contained particles with approximately 20-nm diameter as measured by DLS after redispersion in water (as an example, Fig. 2 shows overlayed results for ZnSe:Mn, ZnSe and ZnSeS) and sphalerite structure as determined by XRD. The width of the XRD patterns indicate the presence of even smaller particles (diameter well below 10 nm); therefore, the particles used in the electrodes after redispersion in water are agglomerates of a small number of crystalline primary particles. All particles were strongly hydrophilic and could easily be redispersed in (slightly basic) water to prepare electrodes.

In a series with varying ratio of S to Se (up to 1:1) in $Zn(S,Se)$:Mn, the associated shift of the band gap energy from the value in pure ZnS to the one in $ZnS_{0.5}Se_{0.5}$ can easily be seen in the excitation spectra of Mn^{2+} emission (Fig. 3). Excitation proceeds via band/band absorption and
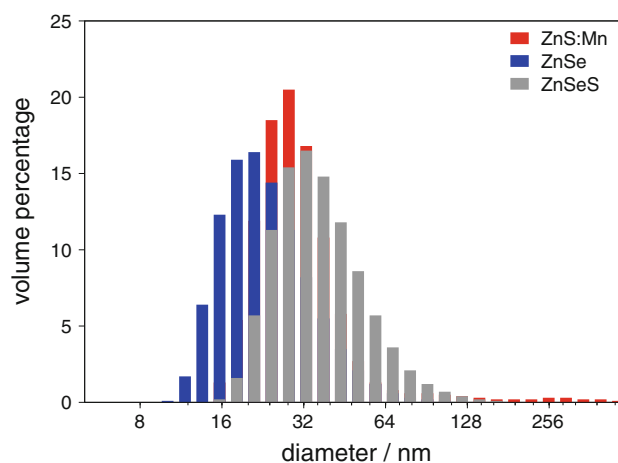

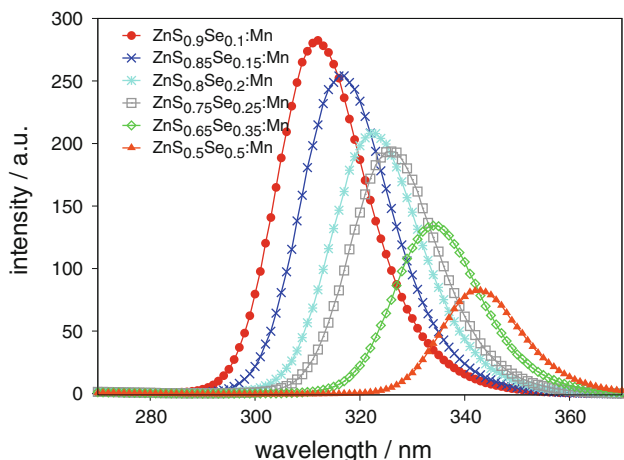**Fig. 2** Particle size of ZnSe:Mn,, ZnSe and ZnSeS as determined by DLS after redispersion in (basic) water

Fig. 3 Excitation spectra monitored at Mn^{2+} emission for various Zn(S,Se) compositions

Fig. 4 V_{oc} for undoped nanoparticles, recorded over time

Fig. 5 V_{oc} for various compositions of Mn-doped nanoparticles, recorded over time

generation of electron/hole pairs; the spectral position of the excitation band thus is a direct measure of the band gap energy. Assuming a constant offset between band gap energy and the maximum of the excitation band, the spectra in Fig. 3 show a decrease of ca. 0.5 eV in the $ZnS_{0.5}Se_{0.5}$ alloy, relative to ZnS, which is in good agreement with the difference in band gap energy of 1.0 eV between pure cubic ZnS and ZnSe. The energy relative to vacuum level of the conduction band edge thus can be decreased by approximately 0.5 eV by alloying of ZnS with ZnSe (using the data from van de Walle and Neugebauer [20]). It can be concluded from these and related data that all particles used in the electrodes are of comparable size, crystal quality and homogeneity. Upward shifts of the conduction band edge by confinement effects (Eq. 1) are expected to be on the order of maximal 0.3 eV, assuming primary particle sizes not less than 5 nm; at this size, the band gap energy of ZnS is approximately 4 eV (bulk value: 3.7 eV).

With the oxidative counter electrode used in the present experiments (standard potential of +0.77 V), maximum cell potentials on the composite electrode are expected to be −0.67 V in case of full mineralization of ethanol to CO_2 and H_2O or at least −0.53 V for reduction of ethanol to acetaldehyde. Figure 4 shows that with electrodes fabricated from pure ZnSe particles, values for V_{oc} of −0.35 to −0.4 V have been reached; therefore, considerable overvoltages are still observed. Without the presence of Zn(S,Se) nanoparticles there is no electrocatalytic activity, as demonstrated by measurements on electrodes made from ITO-coated glass, mixtures of pure carbon paste and activated carbon on glass or pure carbon paste on ITO-coated glass. Electrodes made from pure ZnS- or $Zn_{0.5}Se_{0.5}$- nanoparticles also yielded low values for V_{oc}.
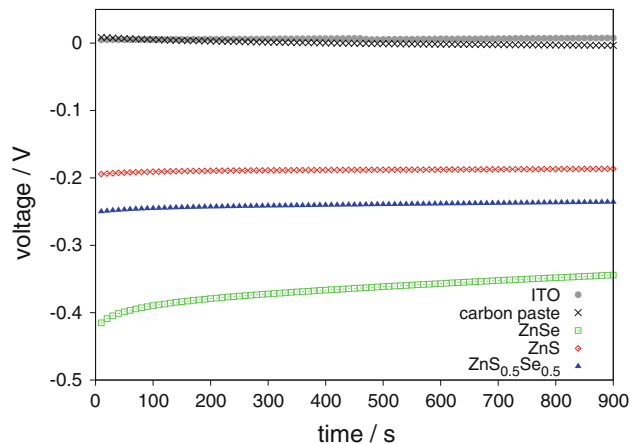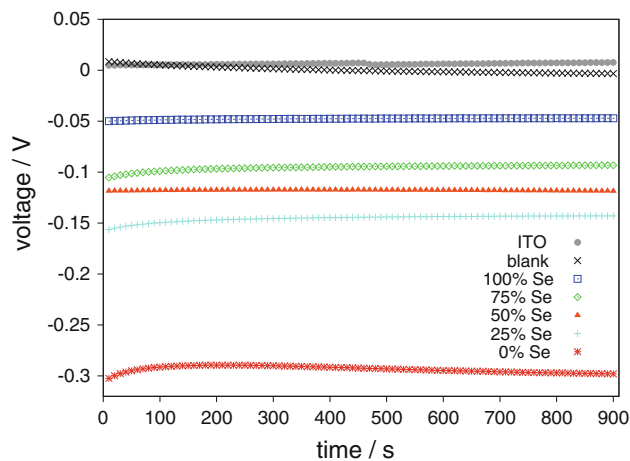
In the case of Mn-doped nanoparticles, the trend observed in Fig. 4 is reversed: now V_{oc} of electrodes with pure ZnS is largest, and alloying with ZnSe considerably reduces V_{oc} (Fig. 5). The presence of Mn^{2+} (most probably also on the particle surface) thus definitely has an influence on the electrocatalytic activity of the electrodes. In optical materials, these surface defects are known to act as quenching sites, which can be removed at least partially by overcoating [25]. The energy levels of these defects thus will be situated in the band gap, and therefore they are expected to accept or trap electrons from adsorbed species in competition with the conduction band, leading to a generally negative influence on the electrocatalytic performance.

In contrast to measurements of V_{oc}, operation of the fuel cell in short-circuit mode delivers the maximal current that can be drawn; barriers like the small membrane between the half cells will limit this current as well as the reaction rate on the electrodes. Figure 6 shows values for I_{sc}

observed under these conditions for electrodes with undoped particles; as in Fig. 4 electrodes with pure ZnSe nanoparticles yield the best results. The current continuously decreases with time, but can be increased again by injections of ethanol. Without Zn(S,Se) nanoparticles, no current is observed (as shown by blanks made from ITO-covered glass or carbon paste on Cu, respectively).

Electrodes with Mn^{2+}-doped nanoparticles yield slightly smaller values for I_{sc} with reversed trend (Fig. 7): ZnS:Mn nanoparticles now yield the best results, as in Fig. 5. Again, the current is slightly decreasing with time, but is increasing again upon ethanol injection.

The morphology of the powders does not change very much during use of the electrodes. Figure 8 shows electron micrographs with examples of a dried ZnSe:Mn powder after synthesis (agglomerates of ca. 20–30 nm with a tendency to form leaf-like superstructures), as well as a used
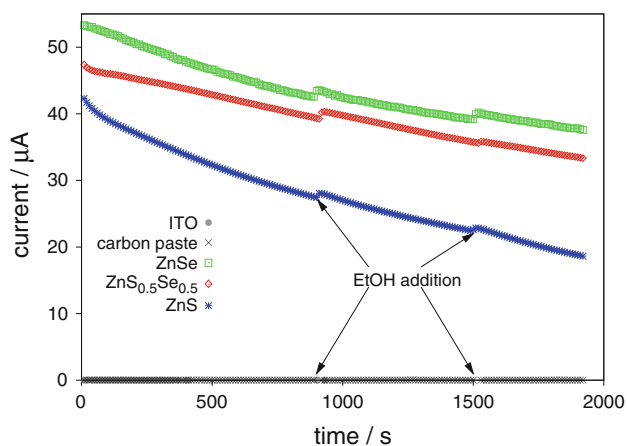

Fig. 6 I_{sc} for undoped nanoparticles, recorded over time, with intermittent addition of ethanol
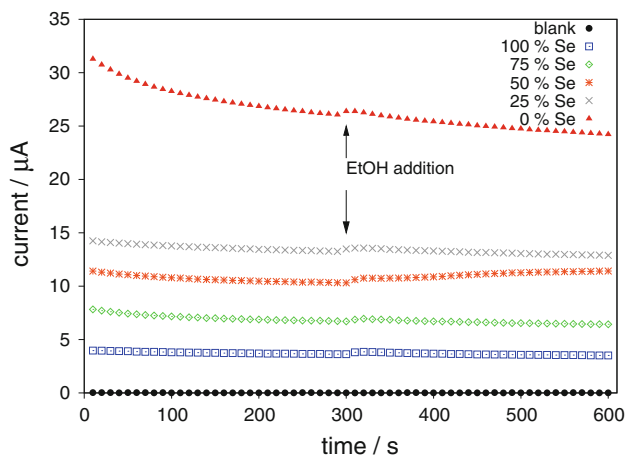

Fig. 7 I_{sc} for various compositions of Mn-doped nanoparticles, recorded over time, with intermittent addition of ethanol

electrode with Zn(S,Se) and a larger area of a used electrode with ZnS:Mn. From the micrographs it is obvious that a part of the Zn(S,Se) is not well connected to the carbon carriers and thus can not exchange charge carriers effectively; therefore, the formation procedure of the Z(S,Se)/ nanocomposites offers large room for improvement of the present cells.

Although the action of Zn(S,Se)-nanoparticles as electrocatalysts and the influence of the Se/S ratio is clearly demonstrated in the experiments presented, and the detailed mechanism is not obvious. An explanation might be found in favourable alignment of the conduction band edge of Zn(S,Se) nanoaparticles and the HOMO level of adsorbed ethanol, since electrons have to pass from adsorbed ethanol molecules to the electrodes during the oxidation process. This would be similar to the mechanism proposed in hybrid bulk heterojunctions for polymer photovoltaic cells. In such a case, small shifts in the position of the conduction band edge may have large influence on the transfer probability and thus the electrocatalytic action. On the other hand, the role of Mn^{2+} at the surface is less clear. Apart from being present as an electronic surface defect site, Mn can occur in several oxidation states and therefore has the potential to facilitate charge transfer beyond being a substitutional defect in Zn(S,Se). Moreover, effects of surface reconstruction in the electrode and after adsorption of ethanol are unclear as well. Future study therefore will have to address these issues, e.g. by modelling of the energetic relations at the interface between the Zn(S,Se) surface and adsorbed ethanol or other potential fuels. Concerning the influence of dopants, it will be interesting to look for other elements than Mn that might even improve the electrocatalytic potential of the nanoparticles. For undoped particles, pure ZnSe seems to perform better than pure ZnS, but unfortunately is chemically not as stable as ZnS, especially against oxidation.

Conclusions

Nanocomposites from carbon and Mn-doped or undoped Zn(S,Se) with various ratios of Se/S have been prepared and tested as electrocatalysts in a fuel cell consuming ethanol. With decreasing Se-content, V_{oc} as well as I_{sc} are increasing in the case of Mn^{2+}-doped nanoparticles, whereas undoped particles show the opposite trend. The highest values observed so far for the cell potential (with electrodes containing either ZnS:Mn or pure ZnSe nanoparticles) are corresponding to about 50% of the thermodynamic standard potential of the cell—the electrocatalysts therefore still are far from being perfect, and further study is needed to increase the conversion rate before practical applications might be envisaged.
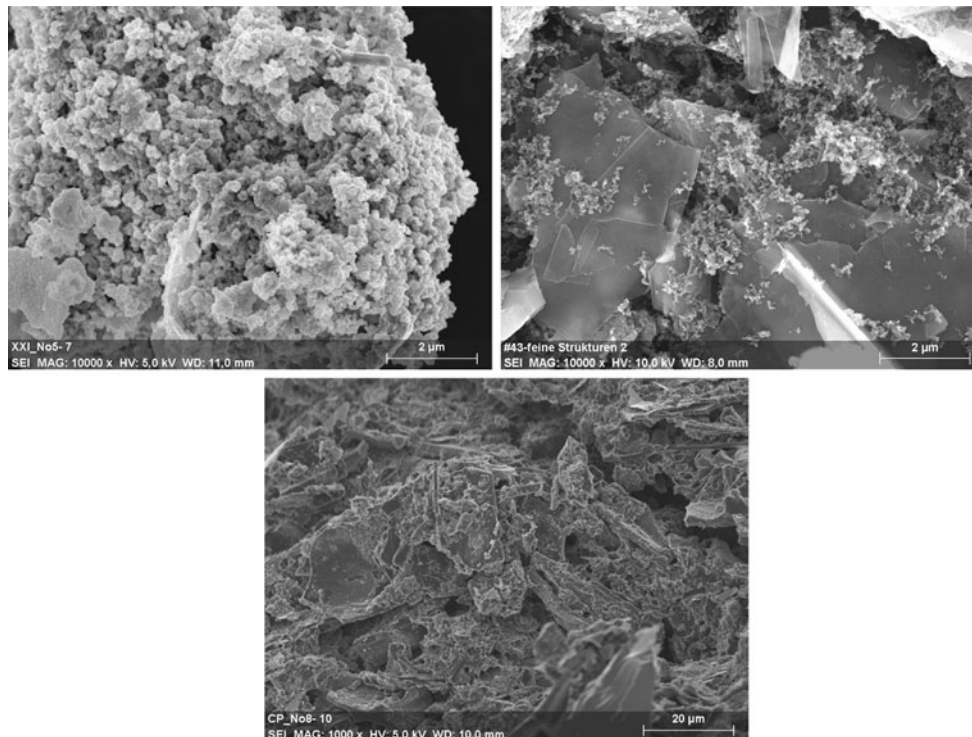
Fig. 8 Electron micrographs of dried ZnSe:Mn powder (*upper left*, scale bar 2 μm), a fractured ZnSeS-containing electrode (*upper right*, scale bar 2 μm) and a ZnS:Mn-containing electrode (*bottom*, scale bar 20 μm)

References

1. Klausch A, Althues H, Schrage C, Simon P, Szatkowski A, Bredol M, Adam D, Kaskel S (2010) J Lumin 130:692. doi:10.1016/j.jlumin.2009.11.021
2. Bredol M, Matras K, Szatkowski A, Sanetra J, Prodi-Schwab A (2009) Sol Energy Mater Sol Cells 93(5):662. doi:10.1016/j.solmat.2008.12.015
3. Yang P, Szatkowski A, Bredol M (2009) J Sol–Gel Sci Technol 51(3):306. doi:10.1007/s10971-009-1979-1
4. Hebalkar N, Lobo A, Sainkar S, Pradhan S, Vogel W, Urban J, Kulkarni S (2001) J Mater Sci 36:4377. doi:10.1023/A:1017910131081
5. Zhang WH, Shi JL, Chen HR, Hua ZL, Yan DS (2001) Chem Mater 13:648
6. Matras K, Bredol M, Szatkowski A, Sakhno O, Stumpe J, Bogdal D (2008) Mol Cryst Liq Cryst 485:28
7. Althues H, Palkovits R, Rumplecker A, Simon P, Sigle W, Bredol M, Kynast U, Kaskel S (2006) Chem Mater 18:1068
8. Wang C, Gao X, Ma Q, Su X (2009) J Mater Chem 19:7016. doi:10.1039/b909546b
9. Hu JS, Ren LL, Guo YG, Liang HP, Cao AM, Wan LJ, Bai CL (2005) Angew Chem Int Ed 44(8):1269
10. Fujiwara H, Hosokawa H, Murakoshi K, Wada Y, Yanagida S (1998) Langmuir 14:5154
11. Wang C, Ao Y, Wang P, Zhang S, Qian J, Hou J (2010) Appl Surf Sci 256:4125. doi:10.1016/j.apsusc.2010.01.095
12. Taghvaei V, Habibi-Yangjeh A, Behboudnia M (2010) Physica E 42:1973. doi:10.1016/j.physe.2010.02.023
13. Kowal A, Li M, Shao M, Sasaki K, Vukmirovic M, Zhang J, Marinkovic N, Liu P, Frenkel A, Adzic R (2009) Nat Mater 8:325. doi:10.1038/NMAT2359
14. Mann J, Yao N, Bocarsly AB (2006) Langmuir 22:10432
15. Nanda J, Sapra S, Sarma D, Chandrasekharan N, Hodes G (2000) Chem Mater 12:1018
16. Bredol M, Kaczmarek M (2010) J Phys Chem A 114(11):3950. doi:10.1021/jp907369f
17. McCreery RL (2008) Chem Rev 108:2646
18. Brus LE (1984) J Chem Phys 80(9):4403. doi:10.1063/1.447218
19. Jasieniak J, Pacifico J, Signorini R, Chiasera A, Ferrari M, Martucci A, Mulvaney P (2007) Adv Funct Mater 17:1654. doi:10.1002/adfm.200600955
20. Van de Walle CG, Neugebauer J (2003) Nature 423:626
21. Zhuang J, Zhang X, Wang G, Li D, Yang W, Li T (2003) J Mater Chem 13:1853
22. Rogach A, Kornowski A, Gao M, Eychmüller A, Weller H (1999) J Phys Chem B 103:3065. doi:10.1021/jp984833b
23. Rogach A, Katsikas L, Kornowski A, Su D, Eychmüller A, Weller H (1996) Ber Bunsenges Phys Chem 100:1772
24. Du J, Fu L, Liu Z, Han B, Li Z, Liu Y, Sun Z, Zhu D (2005) J Phys Chem B 109:12772
25. Xiao Q, Xiao C (2008) Opt Mater 31(2):455. doi:10.1016/j.optmat.2008.06.010